Investigating the combined use of differential SAR tomography and PSI for spatio-temporal inversion

Muhammad A. Siddique
Earth Observation & Remote Sensing
ETH Zurich
Switzerland

Irena Hajnsek
Earth Observation & Remote Sensing,
ETH Zurich, Switzerland
German Aersospace Center - DLR, Germany

Urs Wegmüller
Gamma Remote Sensing AG
Switzerland

Othmar Frey
Earth Observation & Remote Sensing
ETH Zurich
Gamma Remote Sensing AG
Switzerland

***Abstract*—Persistent Scatterer Interferometry (PSI) inherently assumes a single temporally coherent scatterer inside a range-azimuth resolution cell. This restriction leads to the rejection of numerous persistent scatterer (PS) candidates, particularly in urban areas where layovers occur frequently. Moreover, in case of high-rise buildings, it is necessary to compensate the phase associated with thermal expansion in an iterative way. It is worthwhile to approach tomographic techniques to address these concerns. SAR tomography has the potential to separate scatterers in elevation, thus resolving layover. Differential SAR tomography additionally allows retrieval of deformation parameters, including a possible thermal expansion term. In this paper, we investigate the combined use of SAR tomographic approaches and PSI for elevation and deformation estimation. Results are presented for an interferometric time-series of 50 TerraSAR-X stripmap images acquired over Barcelona city. Spatio-temporal inversion of scatterers along the façade of a high-rise building is presented as a special case.**

I. Introduction

Persistent scatterer interferometry (PSI) [1], [2] is a widely used for measurement of slow deformations. It entails identification of the so-called persistent scatterers (PSs), whose behavior ideally corresponds to coherent point targets. In general, it is challenging to locate such scatterers. Any multiplicity of scatterers (such as in a ground-façade layover) inside the same resolution cell restricts point-like behavior; therefore, a conventional PSI candidate selection process rejects it. This may result in limited deformation sampling. In case of urban areas, although generally a good density of PSs is expected due to the presence of numerous man-made structures, but at the same time, layovers are frequent. In particular, high-rise buildings suffer from strong layovers, and thus PSI alone may not be able to provide sufficient deformation sampling for such buildings. PSI and SAR tomography both utilize an interferometric stack of SAR images; while the former estimates the deformation in radar line-of-sight (LOS), the latter estimates the reflectivity along the direction perpendicular to the line-of-sight (PLOS or elevation) using aperture synthesis and/or spectral estimation techniques [3], [4], [5]. SAR tomography thus separates individual scatterers in layover [6] . In this paper, we investigate the combined use of SAR tomography and PSI, extending the ideas presented in [7] [8].

In case of high-rise buildings, it may additionally be necessary to consider a possible temperature-dependent displacement [9] of the scatterers along the building, else it leads to de-focusing in case of tomography and a likely rejection as PS during the PSI candidate selection processing. The uncompensated phase acts as phase noise. Multidimensional SAR tomographic techniques can be employed to model this phase term. At the same time, it can also provide an estimate of the average deformation rate of the scatterer similar to the end-product of a PSI processing.

In this paper, we extend a preliminary PSI analysis with tomography, and discuss the impact of using extended phase models for tomographic inversion. This paper aims to cover the gap by providing a preliminary investigation in this direction.

II. Differential SAR Tomography

The mathematical model for SAR tomography (3D SAR imaging) can be written for a stable point target source for each range-azimuth pixel as [4], [10]:

$$y_n = \int_{\triangle s} \gamma(s) \exp\left[-j\varphi_n(s)\right] \mathrm{d}s \tag{1}$$

where y_n is the n^{th} single-look-complex (SLC) value from a coregistered stack containing N images, $n = 0, 1, \ldots, N-1$, $\gamma(s)$ is the reflectivity profile along the elevation s, and φ_n is the following interferometric phase term:

$$\varphi_n(s) = 2k \triangle r_n(s). \tag{2}$$

k is the central wavenumber, and $\triangle r_n(s)$ can be approximated as [4]:

$$\begin{aligned} \triangle r_n(s) &= r_n(s) - r_0(s) \\ &\approx \frac{s^2}{2\left(r_0 - b_n^{\parallel}\right)} - \frac{b_n^{\perp} s}{r_0 - b_n^{\parallel}}. \end{aligned} \tag{3}$$

r_n is the range distance from sensor *n* to scatterer at elevation *s*, and $b_n^{\perp}$ and $b_n^{\parallel}$ represent the orthogonal and parallel baselines extended by sensor *n*, respectively. Here we consider $n = 0$ as the master in the interferometric stack.

The phase model as in eq. (2) assumes a stationary scatterer. If a linear deformation over time is assumed, the following phase term should be considered instead:

$$\varphi_n(s, \nu) = 2k\left[\triangle r_n(s) + \nu t_n\right] \tag{4}$$

978-1-4799-6652-3/15/$31.00

where ν is the average deformation velocity. The corresponding tomographic model (also know as differential tomography [11]) is

$$y_n = \iint\limits_{\triangle s, \triangle \nu} \gamma(s,\nu) \exp\left[-j\varphi_n(s,\nu)\right] \mathrm{d}s\mathrm{d}\nu \tag{5}$$

In case of thermal expansion induced phase change, the model can be further extended to:

$$\varphi_n(s,\nu,\kappa) = 2k\left[\triangle r_n(s) + \nu t_n + \frac{1}{2k}\kappa\tau_n\right] \tag{6}$$

where τ_n are the local temperatures corresponding to the time of image acquisition, and κ represents the phase-to-temperature sensitivity which would tend to vary for each resolution cell (depending upon material and/or physical structure). The tomographic model can now be concisely written as:

$$y_n = \int\limits_{\triangle \mathbf{p}} \gamma(\mathbf{p}) \exp\left[-j\varphi_n(\mathbf{p})\right] \mathrm{d}\mathbf{p} \tag{7}$$

where $\mathbf{p} = [s, \nu, \kappa]$ is the vector of the parameters to be estimated. Various inversion methods have been proposed (such as [3], [7], [12], [6]). It is not the scope of this paper to compare the different methods; instead the straight-forward conventional beamforming is used. The estimated reflectivity is given by,

$$\hat{\gamma}(\mathbf{p}) = \mathbf{a}^H(\mathbf{p})\,\mathbf{y} \tag{8}$$

where $\mathbf{y}$ is the column vector containing the SLC values, and $\mathbf{a}$ is the steering vector:

$$\mathbf{a}(\mathbf{p}) = \left[\begin{array}{cccc} 1 & e^{-j\varphi_1(\mathbf{p})} & \ldots & e^{-j\varphi_{N-1}(\mathbf{p})} \end{array}\right]^{\mathrm{T}} \tag{9}$$

III. Phase Calibration & PSI

Prior to tomographic inversion, it is necessary to perform a preliminary PSI analysis to obtain precise phase calibration of the interferometric data stack. Atmospheric phase screen (APS) has to be estimated and subsequently removed from each layer in the stack. An accurate estimation of APS is restricted by the presence of various sources of phase noise, such as temporal and geometric decorrelation, orbital errors, etc. This preprocessing step is also required for PSI. Though there are different PSI implementations (such as [1], [2]), each initially performs a PS candidate selection where the more coherent among other scatterers are selected. These scatterers exhibit 'point-like' behavior. They do not suffer strong decorrelation and are, therefore, suited for the estimation of the APS. Once a point-wise estimation is obtained, the low-frequency spatial behavior of the atmospheric phase allows extrapolation to the surrounding non-PS as well. Besides the APS, topographic and orbital phases are simulated and subtracted from each layer. While PSI continues further analysis on PSs (towards a reliable estimation of deformation of the PSs), tomographic techniques can be extended to non-PS as well. In this way, PSI and tomography substantiate each other.

It is important to mention here that during the PS candidate selection process, scatterers in layover often get rejected, and therefore, a PSI-based deformation estimate for such scatterers is not obtained. Again, a tomographic inversion (differential tomography in this case) can provide a solution. In our work, we obtained a PSI solution using the Interferometric Point Target Analysis (IPTA) [2] framework. During the PS candidate selection process, IPTA observes the temporal variability of the backscatter and spectral diversity for each resolution cell. Layovers cases, especially when none among the interfering scatterers is dominant, would likely get rejected owing to a wider spectral diversity than otherwise.

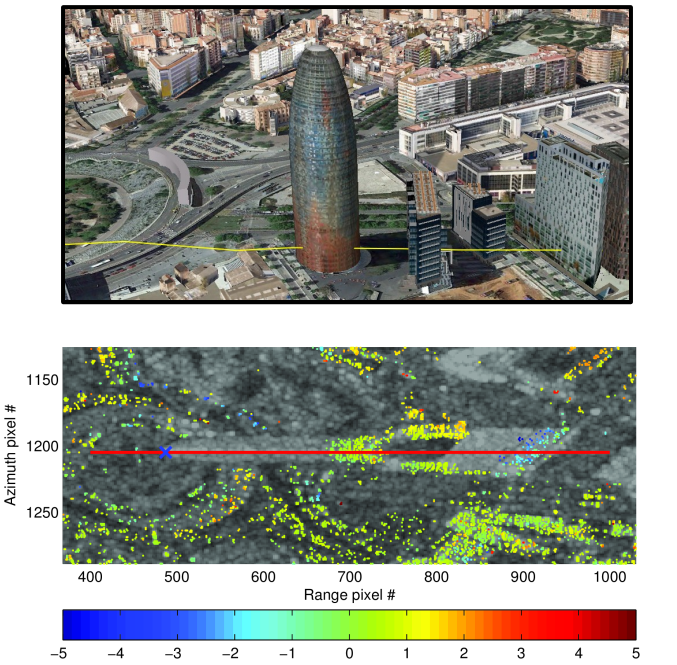

Fig. 1. Top: Google Earth snapshot of the observed area. The yellow line shows the approximate projection of the slant-range vector on ground. Below: An initial PSI solution obtained with IPTA. The dots mark the detected persistent scatterers. Their color represents the estimated deformation in mm/y. The red line shows the extent of an azimuth line whose tomographic inversion is presented afterwards.

IV. Data

An interferometric data stack of 50 TerraSAR-X stripmap acquisitions over the city of Barcelona has been used. The data is multibaseline and multitemporal, acquired over a span of 5 years. The total orthogonal baseline is 503.2 m. With beamforming, we expect the resolution in elevation to be no better than 19 m due to the irregularity of the baselines.

V. Results

The Torre Agbar tower is presented as an example of a high-rise building appearing in layover in the SAR images. Fig. 1 shows a Google Earth snapshot of the tower and the neighborhood. The lower image in the figure is the average SAR backscatter overlaid with colored dots representing PSs. It can be seen that no PS is detected in the upper part of the building. This is expected as the building top is suffering a very strong layover with the nearby ground/roads. However, as it turns out in our investigation, this is not the only reason. We selected a point (non-PS) at the tip of the building (marked with a blue cross in Fig. 1), and performed tomographic inversions for each of the three cases: $\mathbf{p} = [s]$ (P1), $\mathbf{p} = [s, \nu]$

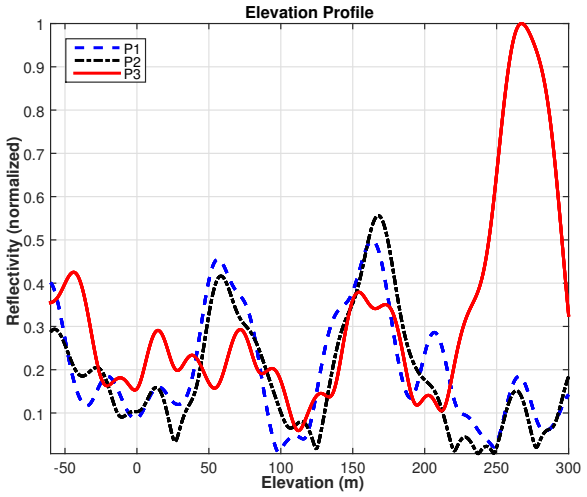

Fig. 2. Elevation profiles obtained for each of the three cases (P1, P2, and P3). The elevation is referenced above SRTM.

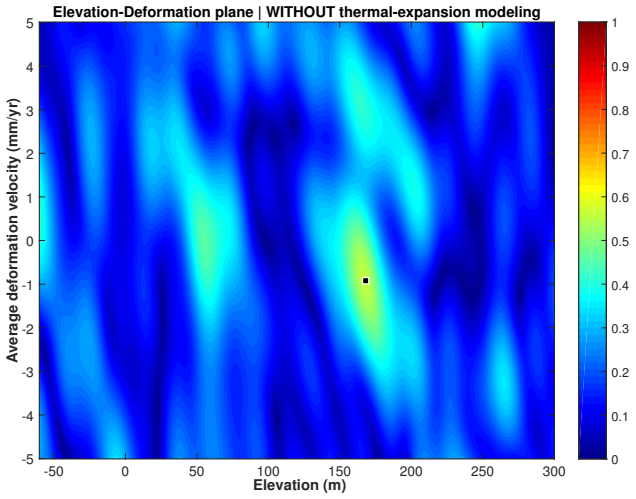

Fig. 3. The elevation-velocity plane, i.e. $|\hat{\gamma}(\mathbf{p})|$ for $\mathbf{p} = [s, \nu]$ (P2). The parameters estimated correspond to the peak location marked in black.

(P2), and $\mathbf{p} = [s, \nu, \kappa]$ (P3). The parameter vector is estimated at the peak of $\hat{\gamma}(\mathbf{p})$.

Fig. 2 shows elevation profiles for each of the three cases. For P1 (i.e. when the phase model does not include deformation and thermal expansion induced phase), the elevation profile shows no well-defined peak. It can be suspected here that the interferometric stack still contains some uncompensated deformation phase. To alleviate this suspicion, we include an average deformation velocity term in the phase model, i.e. P2. The elevation-velocity plane is shown in Fig. 3. The focusing is still not satisfactory. In addition, it can be seen in Fig. 2 (for case P2) that the elevation profile is not well-focused. Only when a thermal expansion induced phase change is modeled, we obtain both a well-focused elevation profile (Fig. 2, P3) as well as a nicely focused peak in the deformation-elevation plane (Fig. 4). This result clearly highlights the importance of appropriate phase modeling. At the same time, it presents the utility of tomographic techniques which allowed a 'simultaneous' retrieval of the unknown parameters. PSI also allows modeling the thermal expansion induced phase; the

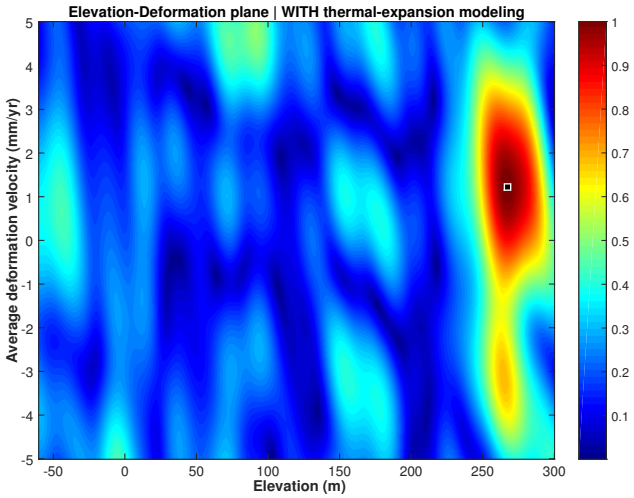

Fig. 4. The elevation-velocity plane, i.e. $|\hat{\gamma}(\mathbf{p})|$ for $\mathbf{p} = [s, \nu, \kappa]$ (P3), with κ fixed to its estimate. The parameters estimated correspond to the peak location marked in black.

average deformation and the phase-to-temperature sensitivity are however obtained in an 'iterative' manner.

Tomographic inversion (case P3) is applied next to all the scatterers along a section of azimuth line (as shown in red in Fig. 1). The estimated scatterer elevation (i.e PLOS distance above the SRTM reference), average deformation velocity and phase-to-temperature sensitivity are shown in Fig. 5. In noisy (low backscatter and/or shadow) regions, the latter two parameters cannot be reliably estimated and the elevation profile remains expectedly unfocused. Applying a threshold on the estimated scatterer reflectivity (normalized) allows us to potentially identify the better-focused scatterers (marked in red). It can be seen that the façade of the building has been properly focused in elevation. The scatterers along the façade have more or less similar average deformation velocity, and rather low, implying overall stability of the building structure. The estimated phase-to-temperature sensitivity is low in magnitude near the base than at the top, which seems plausible as the building top tends to expand/contract more in general with temperature variations.

VI. Conclusion and Outlook

This paper has provided an analysis on the combined use of PSI and SAR tomography with extended phase models. Using a preliminary PSI solution, the interferometric data was phase-calibrated for subsequent tomographic analysis. The results emphasize the importance of appropriate phase modeling. SAR tomographic approaches have the potential to provide a value-addition to PSI in terms of the simultaneous estimation of spatio-temporal parameters associated with both PS and non-PS. The consistency of the deformation results from the two will be investigated in our future work.

Acknowledgement

This research project has been funded by the Swiss Space Office, State Secretariat for Education and Research of the Swiss Confederation (SER/SSO), via the MdP2012 initiative.

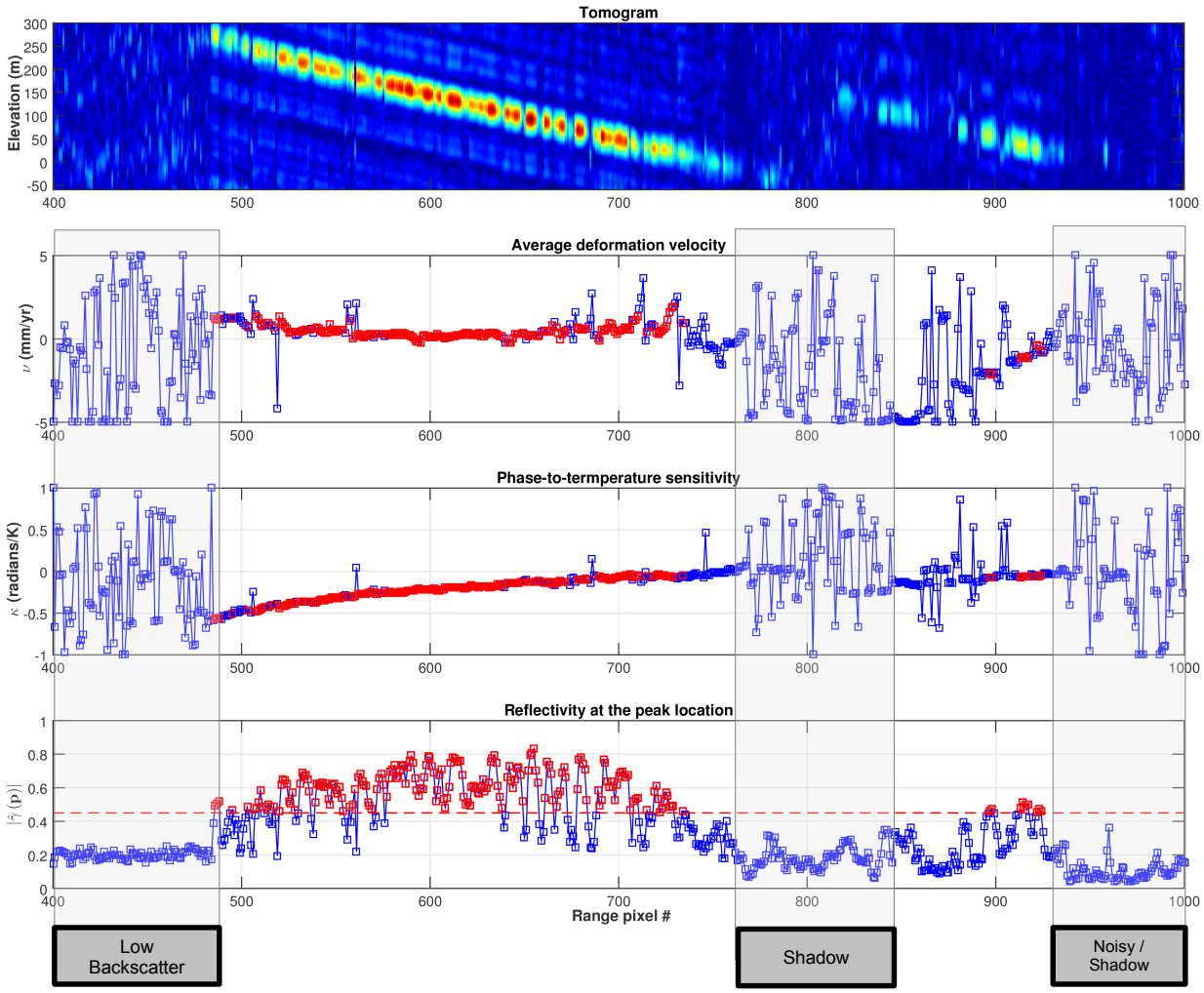

Fig. 5. Results of spatio-temporal inversion with differential tomography (including phase modeling for temperature induced scatterer motion). Top: A tomographic slice along the Torre Agbar building and immediate neighborhood. Bottom: The reflectivity at the peak locations is shown; a simple threshold, marked in dotted-red line, provides discrimination among the noisy and the well-focused scatterers (marked in red). Middle figures: An estimate of the average deformation velocity and the phase-to-temperature sensitivity.

TerraSAR-X SAR data over Barcelona was obtained courtesy of the German Aerospace Center DLR under proposal MTH1717. SRTM is copyright USGS.

REFERENCES

[1] A. Ferretti, C. Prati, and F. Rocca, "Permanent scatterers in SAR interferometry," *IEEE Trans. on Geosc. and Remote Sens.*, vol. 39, no. 1, pp. 8–20, 2001.

[2] C. Werner, U. Wegmüller, T. Strozzi, and A. Wiesmann, "Interferometric point target analysis for deformation mapping," in *Proc. IEEE Int. Geosci. Remote Sens. Symp.*, pp. 4362–4364.

[3] O. Frey, I. Hajnsek, and U. Wegmüller, "Spaceborne SAR tomography in urban areas," in *Proc. IEEE Int. Geosci. Remote Sens. Symp.*, July 2013, pp. 69–72.

[4] G. Fornaro, F. Serafino, and F. Soldovieri, "Three-dimensional focusing with multipass SAR data," *IEEE Trans. on Geosc. and Remote Sens.*, vol. 41, no. 3, pp. 507–517, Mar. 2003.

[5] O. Frey and E. Meier, "3-D time-domain SAR imaging of a forest using airborne multibaseline data at L-and P-bands," *IEEE Trans. on Geosc. and Remote Sens.* , vol. 49, no. 10, pp. 3660–3664, 2011.

[6] F. Lombardini, F. Cai, and D. Pasculli, "Spaceborne 3-D SAR Tomography for Analyzing Garbled Urban Scenarios: Single-Look Superresolution Advances and Experiments," *IEEE Jour. of Sel. Topics in Appl. Earth Observ. and Remote Sens.*, vol. 6, no. 2, pp. 960–968, 2013.

[7] O. Frey, M. Siddique, I. Hajnsek, U. Wegmüller, and C. Werner, "Combining SAR tomography and a PSI approach for high-resolution 3-D imaging of an urban area," in *Proc. 10th European Conf. on SAR*, 2014, pp. 1045–1048.

[8] O. Frey, I. Hajnsek, U. Wegmüller, and C. Werner, " SAR tomography based 3-D point cloud extraction of point-like scatterers in urban areas," in *Proc. IEEE Int. Geosci. Remote Sens. Symp.*, 2014, pp. 1313–1316.

[9] M. Crosetto, O. Monserrat, M. Cuevas-González, N. Devanthéry, G. Luzi, and B. Crippa, "Measuring thermal expansion using X-band persistent scatterer interferometry," *ISPRS Jour. of Photogrammetry and Remote Sens.*, vol. 100, pp. 84 – 91, 2015.

[10] G. Fornaro and F. Serafino, "Imaging of single and double scatterers in urban areas via SAR tomography," *IEEE Trans. on Geosc. and Remote Sens.*, vol. 44, no. 12, pp. 3497–3505, 2006.

[11] F. Lombardini, "Differential tomography: A new framework for SAR interferometry," *IEEE Trans. on Geosc. and Remote Sens.*, vol. 43, no. 1, pp. 37–44, 2005.

[12] X. Zhu and R. Bamler, "Very High Resolution Spaceborne SAR Tomography in Urban Environment," *IEEE Trans. on Geosc. and Remote Sens.*, vol. 48, no. 12, pp. 4296–4308, Dec 2010.